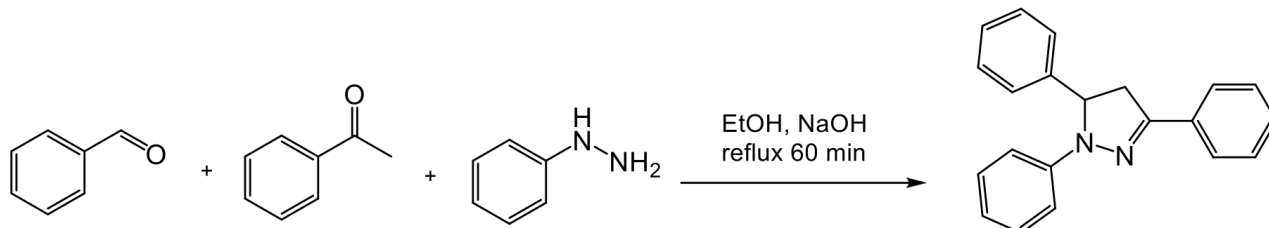


Supporting Information

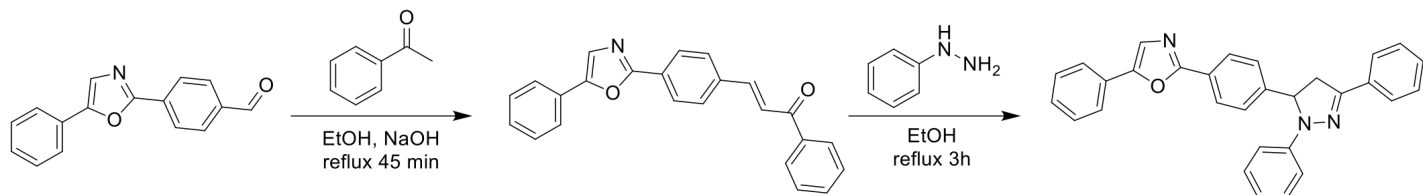
Excited-state dynamics of a molecular dyad with two orthogonally-oriented fluorophores.

Romain Letrun,^{a‡} Bernhard Lang,^a Oleksandr Yushchenko,^a Roland Wilcken,^b Denis Svechkarev,^c Dmytro Kolodieznyi,^{d§} Eberhard Riedle,^b and Eric Vauthey^{*a}

1 Synthesis



PyP. 1,3,5-triphenylpyrazoline was synthesized as described elsewhere.¹ To a mixture of 10 mL of ethanol and 0.5 mL of 10% aqueous NaOH were added acetophenone (1.15 mL, 10 mmol), benzaldehyde (1 mL, 10 mmol), and freshly distilled phenylhydrazine (1.05 mL, 11 mmol). The reaction mixture was then allowed to reflux for 60 minutes. The mixture was then cooled down, filtered and washed with cold ethanol (3x5 mL) to afford white crystals (yield 2 g, 70%). The purity of PyP was checked by comparing the fluorescence excitation and the absorption spectra.



PyOx. A mixture of the phenyloxazole-aldehyde (1g, 4 mmol) and acetophenone (0.468 mL, 4 mmol) in 15 mL of ethanol with 1.93 g of NaOH was refluxed for 45 minutes. Freshly distilled phenylhydrazine (0.434 mL, 4.4 mmol) was added and the mixture refluxed for 3 more hours. Reaction was cooled down, filtered and washed with water. The crude product was recrystallized from toluene to afford off-white crystals (yield 1.3 g, 73%). ¹H NMR (500 MHz, CDCl₃): 3.24 (dd, 1H), 3.96 (dd, 1H), 5.39 (dd, 1H), 6.86 (t, 1H), 7.14 (d, 2H), 7.25 (m, 3H), 7.32 (s, 1H), 7.40 (m, 2H), 7.44-7.52 (m, 5H), 7.76 (d, 2H), 7.80 (d, 2H), 8.14 (d, 2H).

^a Department of Physical Chemistry, University of Geneva, 30 Quai Ernest-Ansermet, CH-1211 Geneva 4, Switzerland. E-mail: eric.vauthey@unige.ch

^b Lehrstuhl für BioMolekulare Optik, Ludwig-Maximilians-Universität München, Oettingenstr. 67, 80538 München (Germany)

^c Department of Pharmaceutical Sciences, University of Nebraska Medical Center, Omaha, Nebraska 68198-6858, United States

^d V.N. Karazin Kharkiv National University, 4 Svobody Square, Kharkiv 61022, Ukraine

‡ Present address: European XFEL GmbH, Holzkoppel 4, 22869 Schenefeld, Germany.

§ Present address: Department of Chemistry, Carnegie Mellon University, Pittsburgh, Pennsylvania 15213, United States.

2 Global Analysis

Global analysis of the time-resolved spectroscopic data, $S(\lambda, t)$, was performed using two approaches.² In the first one:

$$S(\lambda, t) = \sum_l^N A_l(\lambda) \exp(-k_l t), \quad (\text{S1})$$

with $k_l = 1/\tau_l$, where τ_l is the lifetime of component l and $A_l(\lambda)$ its the amplitude. Eq.S1 corresponds to a global multi-exponential analysis. When applying this approach to transient absorption spectra, the $A_l(\lambda)$ are so-called Decay-Associated Difference Spectra (DADS).

In the second approach:

$$S(\lambda, t) = \sum_l^N B_l(\lambda) c_l(t), \quad (\text{S2})$$

where $c_l(t)$ is the time-dependent concentration of species l and $B_l(\lambda)$ its spectrum. As we assume a series of N successive exponential steps, $c_l(t)$ is given by:^{2,3}

$$c_l(t) = \sum_{j=1}^l b_{jl} \exp(-k_j t), \quad (\text{S3})$$

with the amplitudes b_{jl} are $b_{11} = 1$, and for $j \leq l$:

$$b_{jl} = \frac{\prod_{m=1}^{l-1} k_m}{\prod_{n=1, n \neq j}^l (k_n - k_j)}. \quad (\text{S4})$$

Eq.S2-S4 correspond to global target analysis, where the target scheme is a succession of N exponential steps. Formally, the $B_l(\lambda)$ obtained from such an analysis are Species-Associated Difference Spectra (SADS).

Here we use a succession of N exponential steps with increasing time constants in order to visualise the main spectral changes (and their time scale) occurring in the transient absorption data. As the resulting $B_l(\lambda)$ spectra are not attributed to any specific state/species, these spectra are called Evolution-Associated Difference Spectra (EADS) instead of SADS. It should be noted that, for a given value of N , both approaches (eq.S1 or eq.S2) give the same decay constants, k_l . The resulting EADS are linear combinations of the DADS.²

3 Additional Results

3.1 Steady-State Spectroscopy

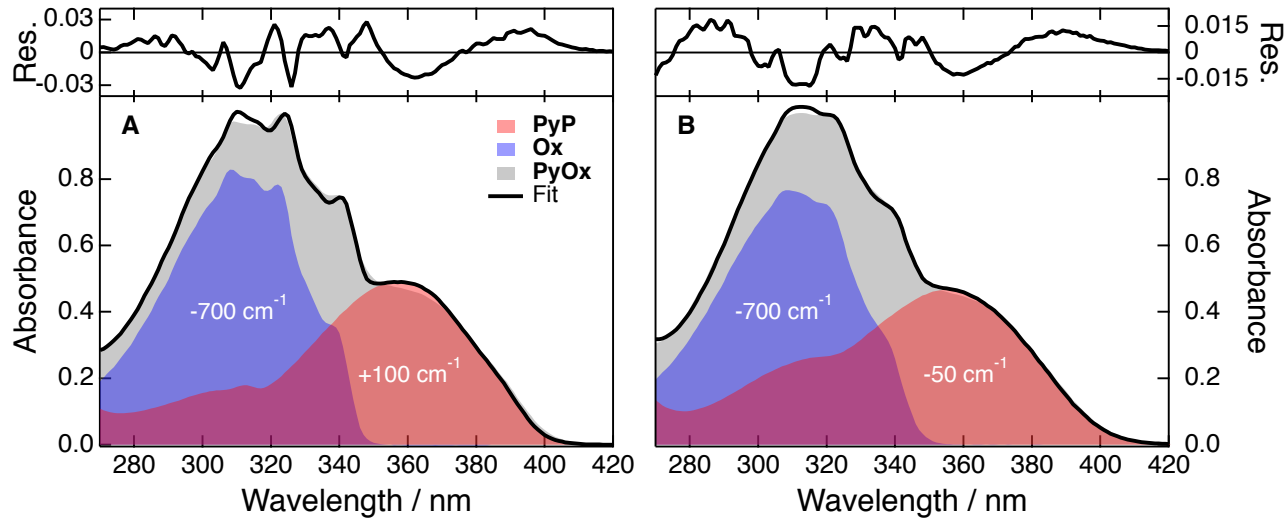


Fig. S1: Absorption spectrum of the **PyOx** reproduced by a linear combination of the spectra of **PyP** and **Ox** in CHX (A) and ACN (B). The scaling factors and shifts (indicated in cm^{-1}) have been optimized by least squares. A negative shift means that the spectrum of the sub-unit had to be red-shifted to reproduce the spectrum of the dyad.

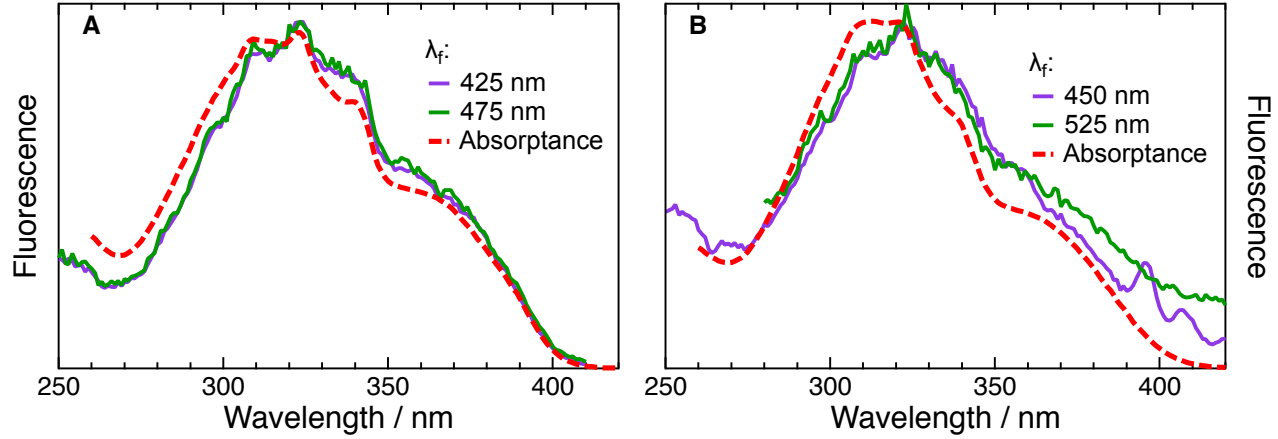


Fig. S2: Excitation spectra recorded with **PyOx** at different emission wavelengths in CHX (A) and ACN (B). The absorptance spectra (red, dashed) were calculated from the absorption spectra shown in Figure S1 scaled to the absorbance used for recording the excitation spectra. Given the small fluorescence quantum yields, especially in ACN, differences between the excitation and absorptance spectra are not significant.

3.2 Transient Absorption

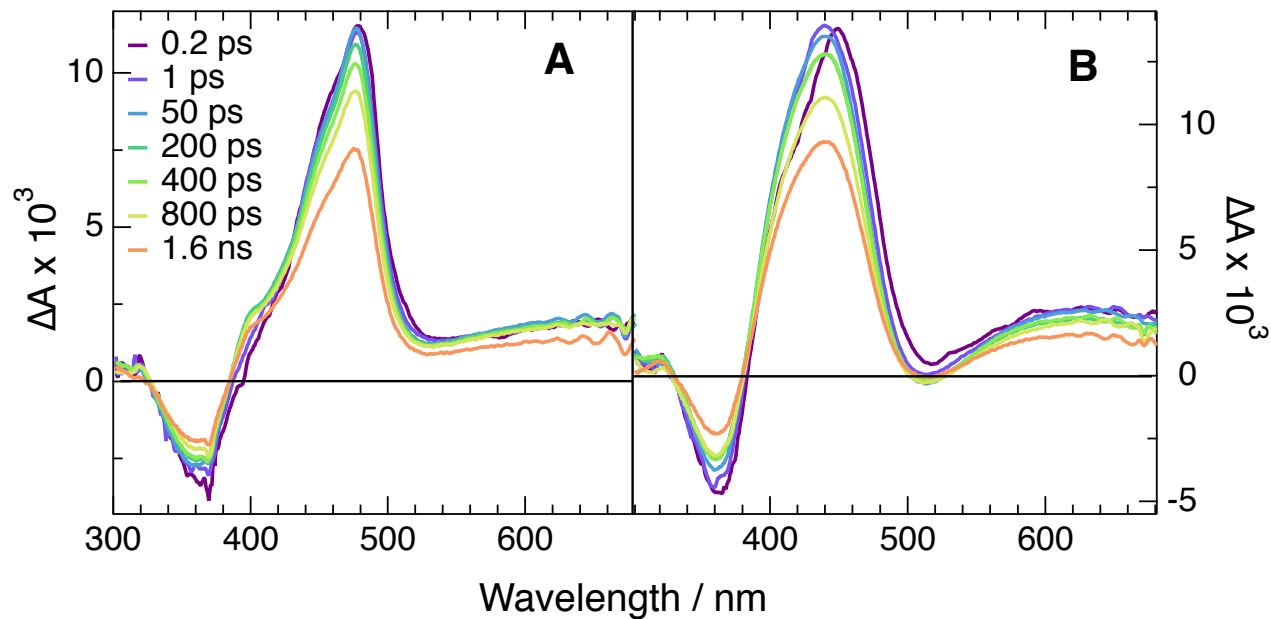


Fig. S3: Transient absorption spectra measured after 370 nm excitation of **PyP** in CHX (A) and ACN (B).

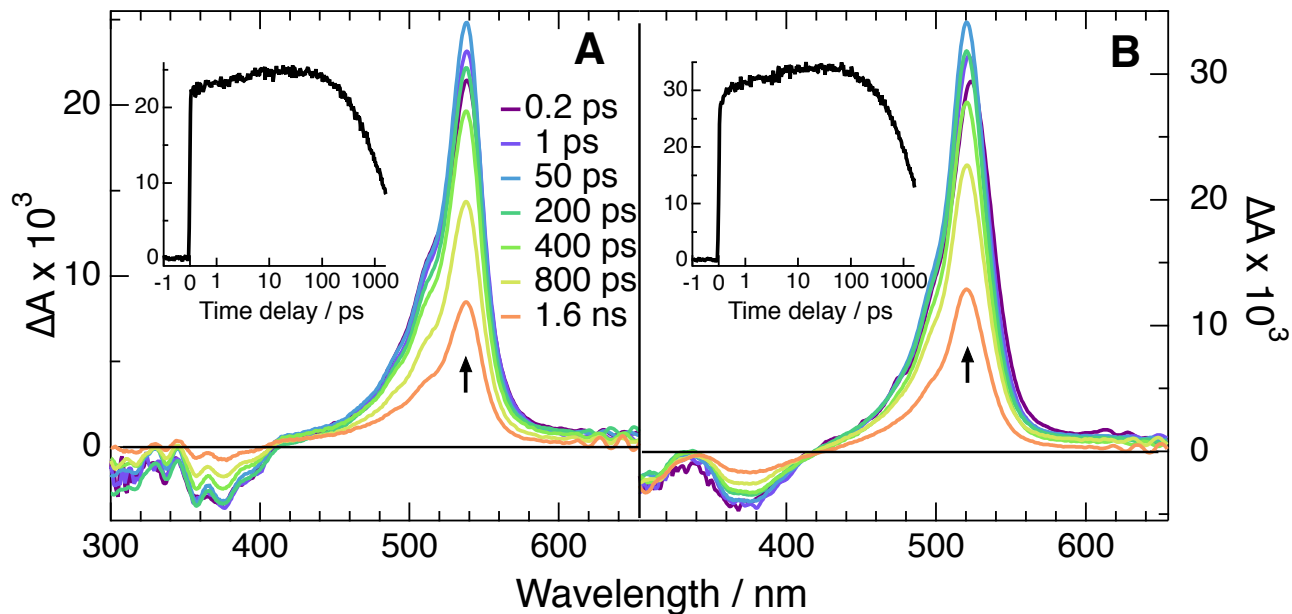


Fig. S4: Transient absorption spectra measured after 325 nm excitation of **Ox** in CHX (A) and ACN (B). Inset: Time dependence at the wavelength indicated by the arrow.

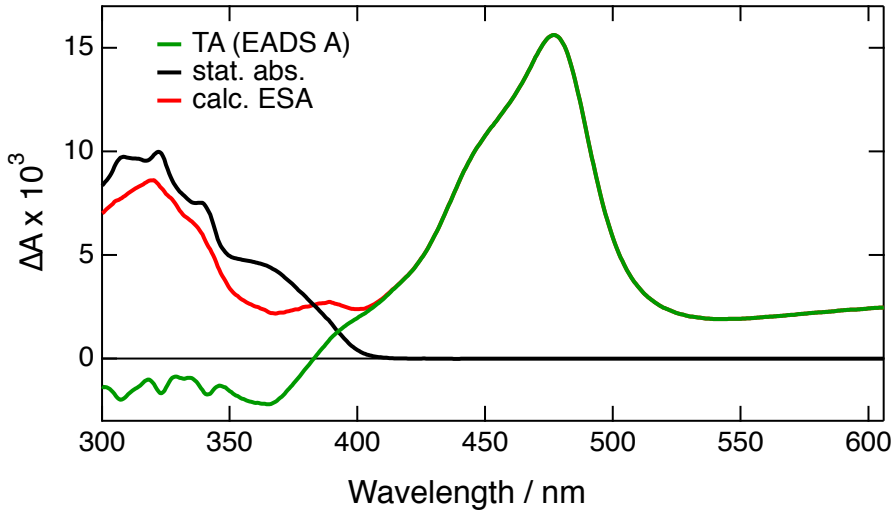


Fig. S5: $S_n \leftarrow S_1$ ESA spectrum of **PyOx** in CHX calculated upon adding the stationary absorption spectrum to the TA absorption spectrum. For better signal/noise ratio, the evolution-associated difference absorption spectrum A obtained from the global analysis of the TA data measured with **PyOx** upon 368 nm excitation (Figure S6D) was used. The ESA spectrum still contains the contribution from the stimulated emission.

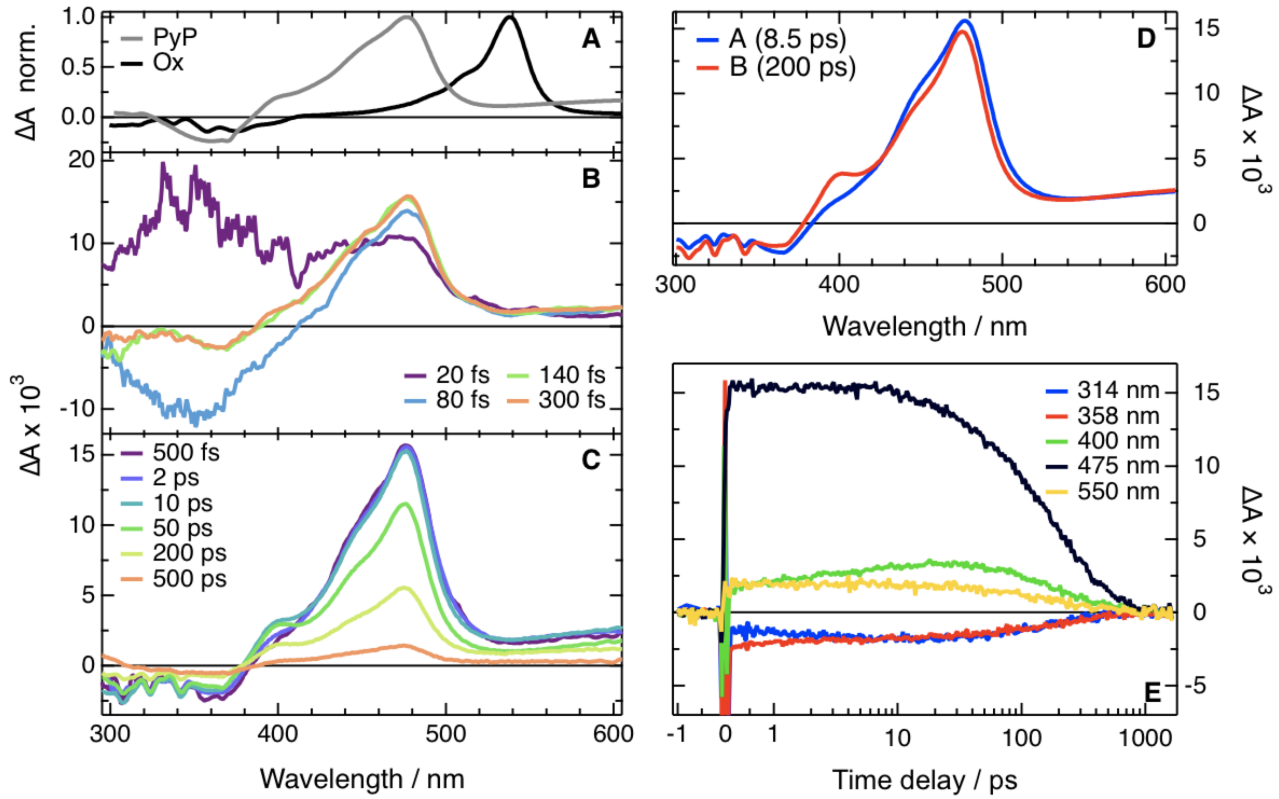


Fig. S6: Long-lived EADS of **PyP** and **Ox** in CHX, for reference (A); TA spectra measured with **PyOx** in CHX upon 368 nm excitation (B-C); Evolution-associated difference spectra obtained from global analysis with two successive steps (D), and time profiles at selected wavelengths (E).

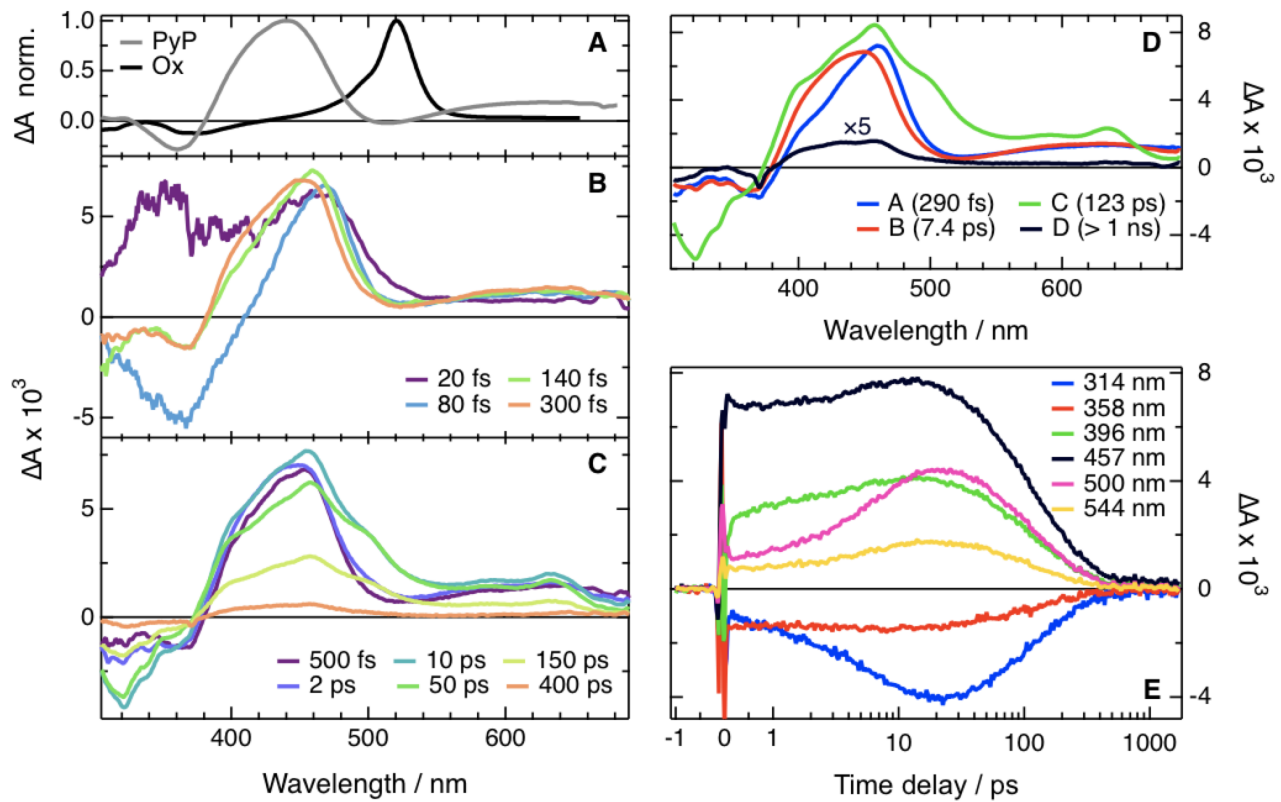


Fig. S7: Long-lived EADS of PyP and Ox in ACN, for reference (A); TA spectra measured with PyOx in ACN upon 368 nm excitation (B, C); evolution-associated difference spectra obtained from global analysis with four successive steps (D), and time profiles at selected wavelengths (E).

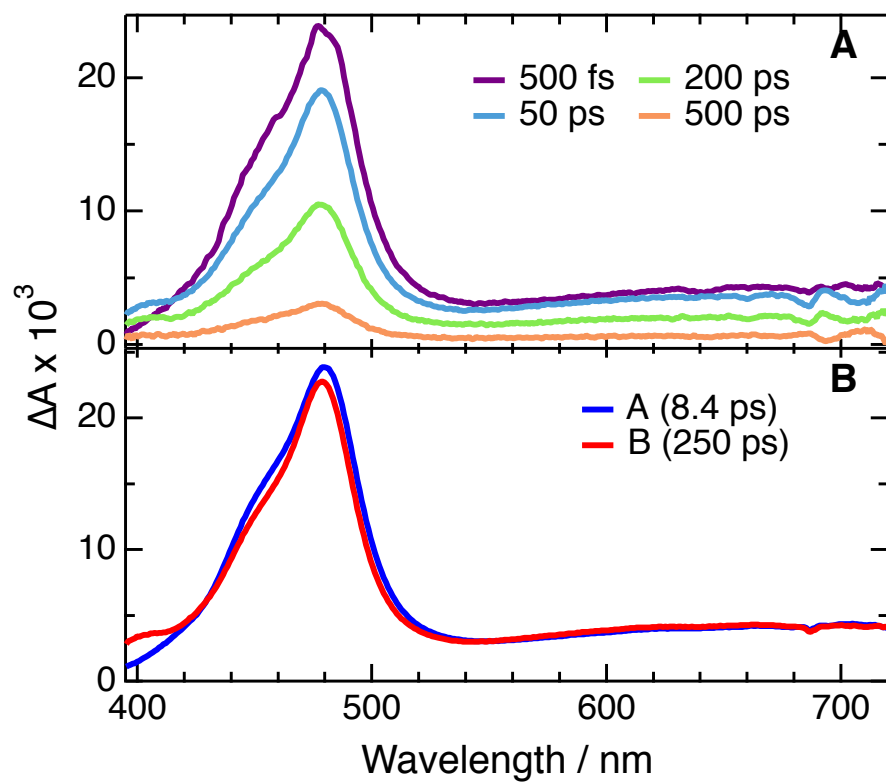


Fig. S8: TA spectra measured with PyOx in decaline after 385 nm excitation (A) and evolution-associated difference spectra obtained from global analysis with two sequential steps (B).

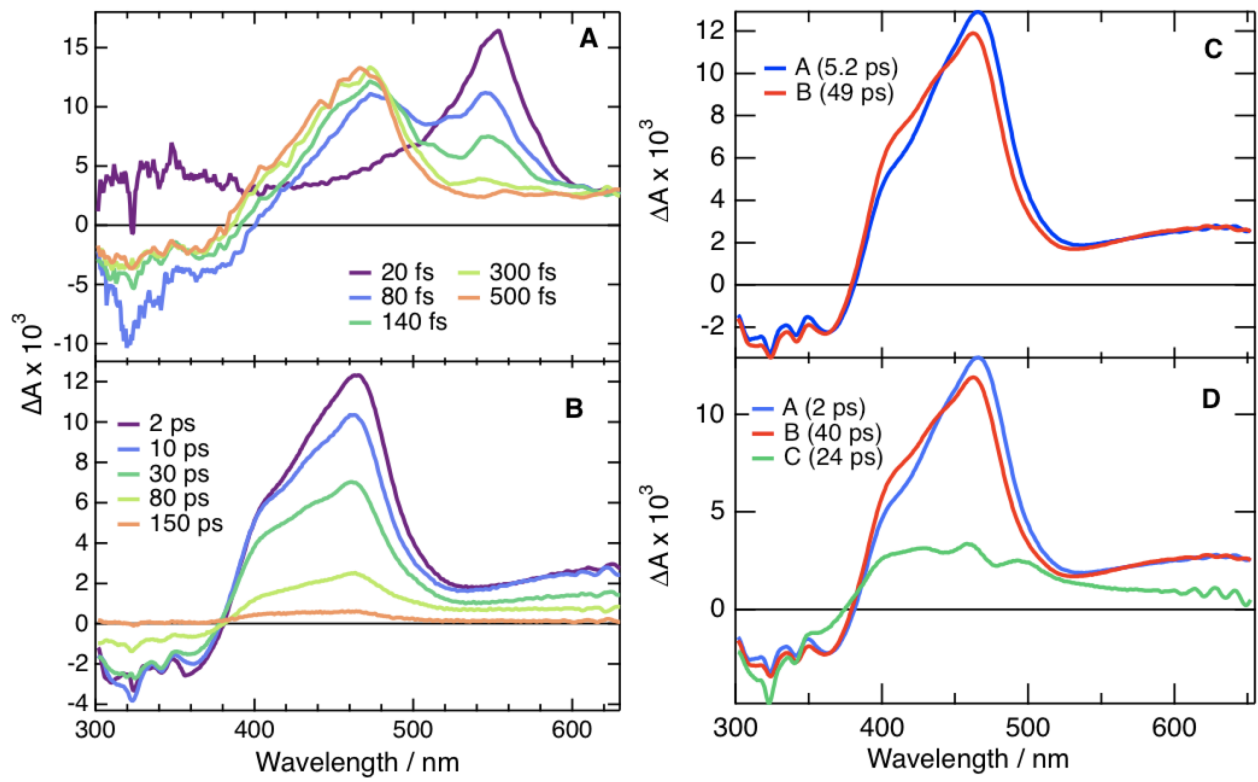


Fig. S9: TA spectra measured with **PyOx** in THF after 321 nm excitation (A,B); evolution/species-associated difference spectra obtained from global analysis of the data after 1 ps using two successive steps (B) and three successive steps with the third step faster than the second one (C).

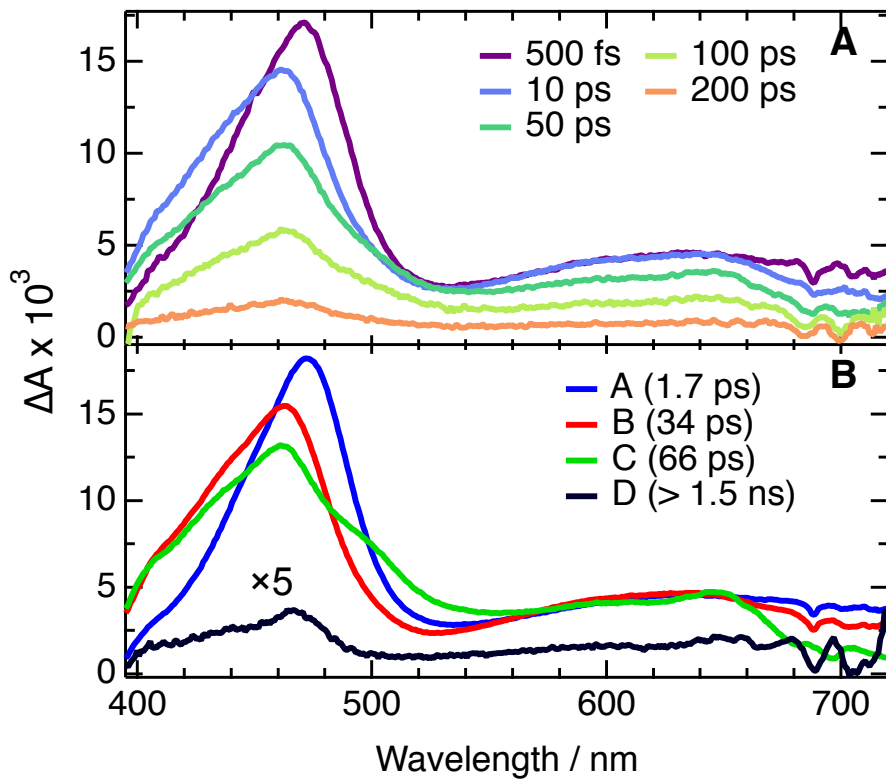


Fig. S10: TA spectra measured with PyOx in dichloroethane after 385 nm excitation (A), and evolution-associated difference spectra obtained from global analysis with four sequential steps (B).

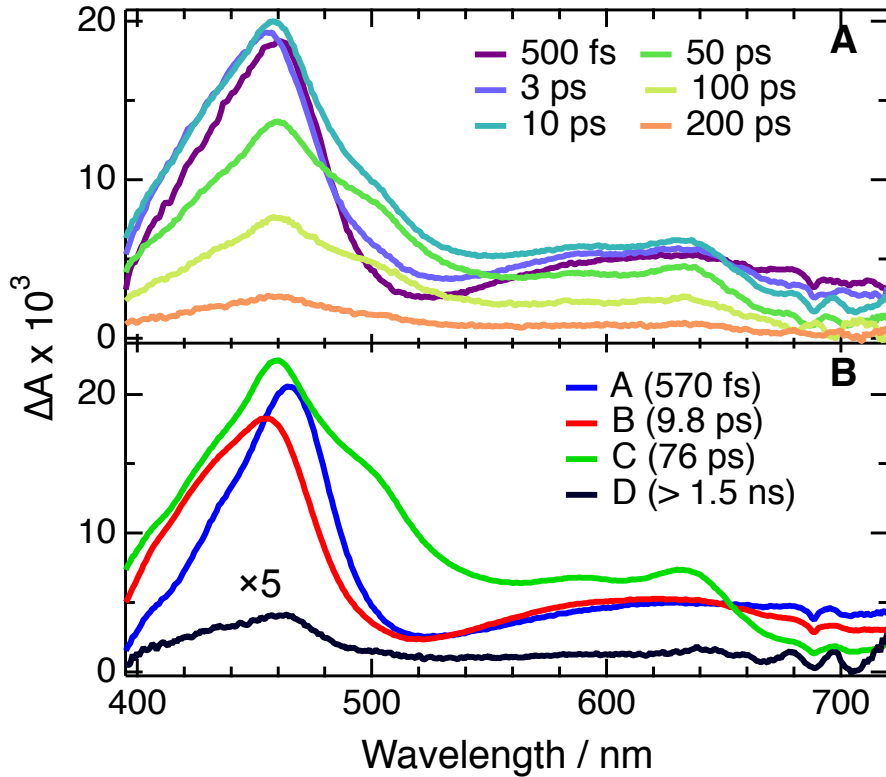


Fig. S11: TA spectra measured with PyOx in acetone after 385 nm excitation (A), and evolution-associated difference spectra obtained from global analysis with four sequential steps (B).

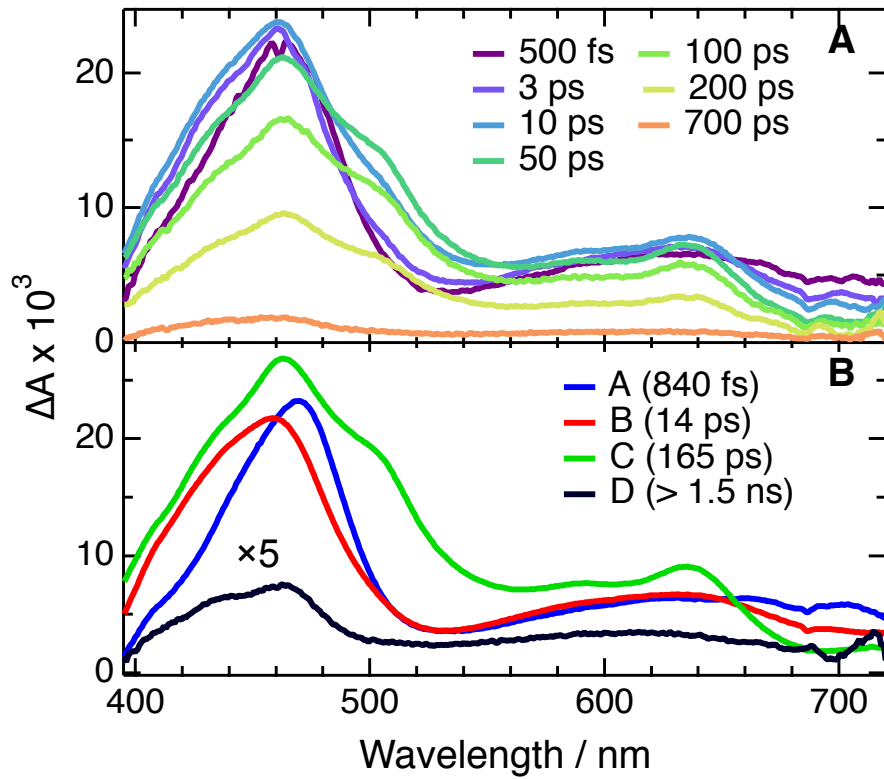


Fig. S12: TA spectra measured with PyOx in DMF after 385 nm excitation (A), and evolution-associated difference spectra obtained from global analysis with four sequential steps (B).

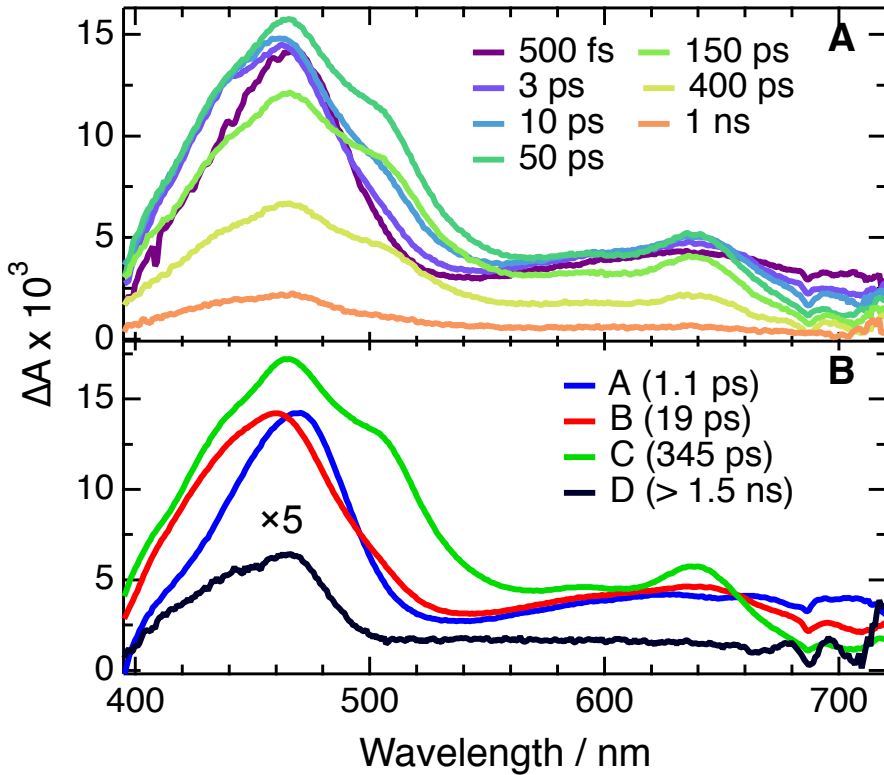


Fig. S13: TA spectra measured with PyOx in DMSO after 385 nm excitation (A), and evolution-associated difference spectra obtained from global analysis with four sequential steps (B).

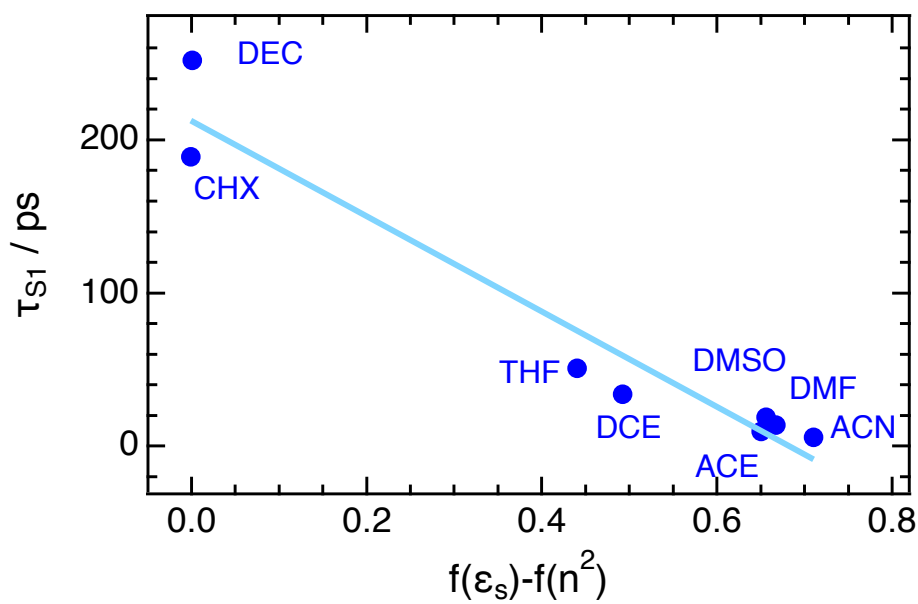


Fig. S14: Dependence of the S_1 state lifetime of **PyOx** on the solvent polarity. The solid line is only to highlight the trend.
 $f(\epsilon_s) - f(n^2) = (\epsilon_s - 1)/(\epsilon_s + 2) - (n^2 - 1)/(n^2 + 2)$.

3.3 Fluorescence in a Polymer Film

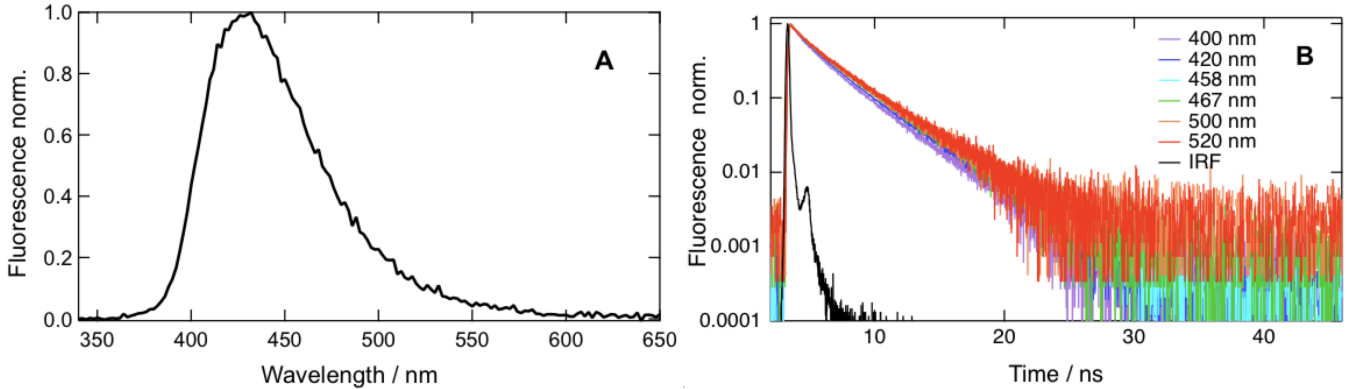


Fig. S15: Fluorescence of **PyOx** in a polyvinylbutyral (PVB) film: stationary spectrum upon 330 nm excitation (A) and time-correlated single-photon counting (TCSPC) profiles upon 375 nm excitation (B). The TCSPC data could be well reproduced with the convolution of the IRF with a biexponential function with a first time constant around 1 ns (0.96 ns at 420 nm, 1.2 at 520 nm, relative amplitude around 0.35) and a second time constant of about 3.5 ns (3.3 ns at 420 nm and 3.8 ns at 520 nm).

4 Energy of the Charge-Separated State

The free energy of charge separation, ΔG_{CS} , and the energy of the charge-separated state, E_{CS} , have been estimated using the Weller equation:⁴

$$\Delta G_{CS} = E_{CS} - E_{00} = e [E_{ox}(D) - E_{red}(A)] - E_{00} + C + S, \quad (\text{S5})$$

where E_{00} is the 0-0 transition energy of the excited state involved in the process, e is the elementary charge, $E_{ox}(D)$ and $E_{red}(A)$ are the oxidation and reduction potentials of the donor and acceptor, respectively. C accounts for the electrostatic interaction between the charged moieties and is defined as:

$$C = -\frac{e^2}{4\pi\epsilon_0\epsilon_s r_{DA}}, \quad (\text{S6})$$

where ϵ_0 is the vacuum permittivity, ϵ_s is the static dielectric constant of the solvent, and r_{DA} is the donor-acceptor distance. The last term in Equation S5 corrects for a different solvent than that used for the measurement of the redox potentials, and is given by:

$$S = -\frac{e^2}{8\pi\epsilon_0} \left(\frac{1}{r_d} - \frac{1}{r_a} \right) \left(\frac{1}{\epsilon_s^r} - \frac{1}{\epsilon_s} \right), \quad (\text{S7})$$

where r_D and r_A are the radii of the donor and acceptor, respectively. The superscript r denotes the reference, i.e., the solvent used for the determination of the redox potentials.

The values used for the calculation are given below. The radii have been estimated from the Van der Waals volume calculated with the increments method,⁵ whereas the donor-acceptor distance has been estimated by taking the distance between the centres of mass of the Py and Ox subunits obtained from the optimized ground-state geometry:

$E_{ox}(\text{PyP}) = 0.89$ V (vs. SCE in DMF)⁶; $E_{red}(\text{PyP}) = -2.32$ V (vs. SCE in DMF)⁶;

$E_{red}(\text{Ox}) = -2.13$ V (vs. SCE in DMF)⁷; $E_{ox}(\text{Ox}) = 1.46$ V (vs. SCE in ACN)⁸;

$E_{00} = 3.09$ eV;

$r_{DA} = 7.8$ Å; $r_D = 4.0$ Å; $r_A = 3.6$ Å.

With these values, eq.S5 gives $\Delta G_{CS} = -0.12$ eV in ACN and +0.8 eV in CHX for the charge separation from **Py** to **Ox**. The driving force for the charge separation from **Ox** to **Py** is predicted to amount to +0.64 eV in ACN.

5 Excitation energy transfer

The rate constant of excitation energy transfer (EET) from the **Ox** to the **Py** moiety of **PyOx** has been estimated using the Förster model.⁹ The EET rate constant, in ps^{-1} , can be expressed in a Golden Rule form:¹⁰

$$k_{EET} = 1.18(\text{ps}^{-1}\text{cm})|V|^2\Theta, \quad (\text{S8})$$

where V is the interaction energy (in cm^{-1}) and Θ is the spectral overlap integral (in cm), obtained from the area-normalized emission and absorption bands of the donor and acceptor, respectively, represented on a wavenumber scale. In the Förster model, V is calculated as the interaction energy between the transition dipole moment of the energy donor, $\vec{\mu}_d$, and that of the acceptor, $\vec{\mu}_a$:

$$V_{dd} = 1.18 \frac{|\vec{\mu}_d||\vec{\mu}_a|f_L^2}{\epsilon_{op}r_{da}^3} \kappa, \quad (\text{S9})$$

where V_{dd} is in cm^{-1} , the transition dipole moments are in D, r_{da} is the distance in nm, $\epsilon_{op} \simeq n^2$ is the dielectric constant at optical frequencies, n is the refractive index, $f_L = (\epsilon_{op} + 2)/3$ is the Lorentz local field correction, and κ is the orientation factor:

$$\kappa = \cos \beta_{da} - 3 \cos \beta_d \cos \beta_a, \quad (\text{S10})$$

with β_{da} the angle between $\vec{\mu}_d$ and $\vec{\mu}_a$, β_d and β_a the angles between the dipoles and \vec{r}_{da} .

The following values, obtained from the optimised ground-state geometry, were used:

$\vec{\mu}_d = 3.2 \text{ D}$ ($S_2 \leftarrow S_0$ transition, localised on **Ox**).

$\vec{\mu}_a = 2.7 \text{ D}$ ($S_1 \leftarrow S_0$ transition, localised on **Py**).

$\beta_{da} = 116.5 \text{ deg.}$; $\beta_d = 8.1 \text{ deg.}$; $\beta_a = 125 \text{ deg.}$; $r_{DA} = 7.8 \text{ \AA}$; $\kappa = 1.24$.

With these values and with $f_L^2/\epsilon_{op} = 0.9$ for CHX and ACN, eq.(S9) gives $V_{dd} = 56 \text{ cm}^{-1}$.

The spectral overlap integral, Θ , between the emission spectrum of **Ox** and the absorption spectrum of **PyP** amounts to $1.43 \cdot 10^{-4} \text{ cm}$. Inserting all these values in eq.(S8) results in a EET rate constant of $k_{EET} = (1.9 \text{ ps})^{-1}$. Alternatively, a EET rate constant of $(100 \text{ fs})^{-1}$ would require a coupling energy of $V = 250 \text{ cm}^{-1}$.

6 Quantum-chemical calculations

Table S1: Transition energy, oscillator strength (f), dominant contributions (or localisation) obtained from the TD-DFT calculations of **PyOx** in the ground and S_1 state geometries. Only the five lowest transitions to triplet states and three lowest transitions to singlet states are listed.

| Transition | Energy / eV | f | dominant contribution (localisation) |
|-----------------------|-------------|------|--------------------------------------|
| Ground-state geometry | | | |
| $T_1 \leftarrow S_0$ | 2.36 | 0 | HOMO→LUMO+1 (Py) |
| $T_2 \leftarrow S_0$ | 2.57 | 0 | HOMO-1→LUMO (Ox) |
| $T_3 \leftarrow S_0$ | 3.26 | 0 | HOMO-1→LUMO+2 (Ox) |
| $T_4 \leftarrow S_0$ | 3.77 | 0 | many (Py) |
| $T_5 \leftarrow S_0$ | 3.86 | 0 | many (Py) |
| $S_1 \leftarrow S_0$ | 4.03 | 0.72 | HOMO→LUMO+1 (Py) |
| $S_2 \leftarrow S_0$ | 4.27 | 1.07 | HOMO-1→LUMO (Ox) |
| $S_3 \leftarrow S_0$ | 4.37 | 0.02 | HOMO→LUMO (CT) |
| S_1 state geometry | | | |
| $T_1 \leftarrow S_0$ | 1.35 | 0 | HOMO→LUMO (CT from Ox) |
| | | | HOMO→LUMO+1 (CT from Py) |
| $T_2 \leftarrow S_0$ | 2.54 | 0 | HOMO-1→LUMO (Ox) |
| | | | HOMO-1→LUMO+1 (CT from Ox) |
| $S_1 \leftarrow S_0$ | 3.18 | 0.50 | HOMO→LUMO (CT from Py) |
| $T_3 \leftarrow S_0$ | 3.23 | 0 | many (Ox) |
| $T_4 \leftarrow S_0$ | 3.31 | 0 | many (Py) |
| $T_5 \leftarrow S_0$ | 3.66 | 0 | many (Py) |
| $S_2 \leftarrow S_0$ | 4.00 | 0.09 | HOMO-1→LUMO (CT from Ox) |
| $S_3 \leftarrow S_0$ | 4.22 | 1.13 | HOMO-1→LUMO+1 (CT from Ox) |

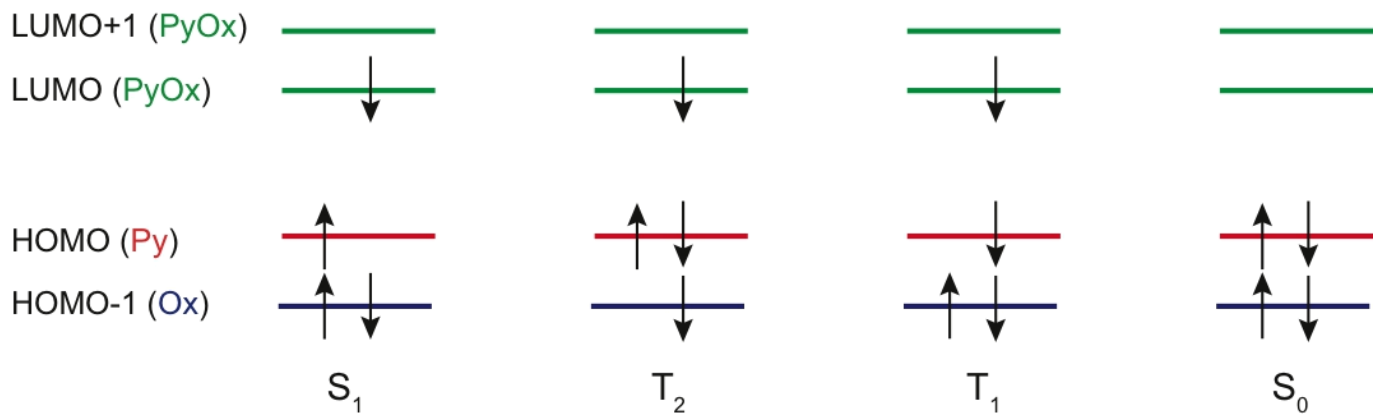


Fig. S16: MO level schemes illustrating the dominant configurations of the lowest electronic states of PyOx at the S_1 state geometry. The MOs are shown in Figure 9 (main text).

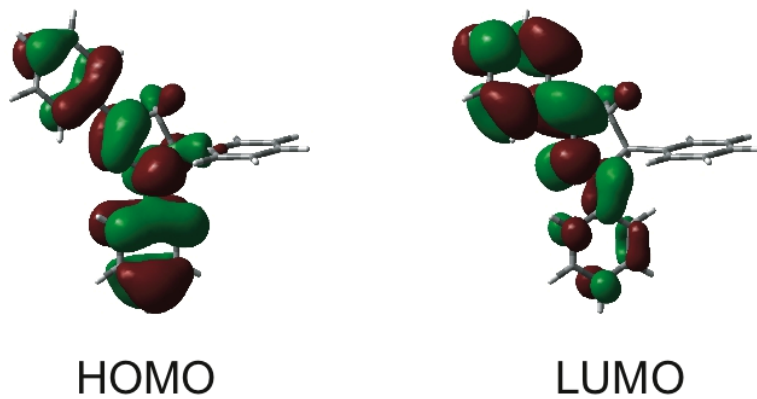


Fig. S17: Frontier molecular orbitals of PyP calculated at the S_1 state geometry.

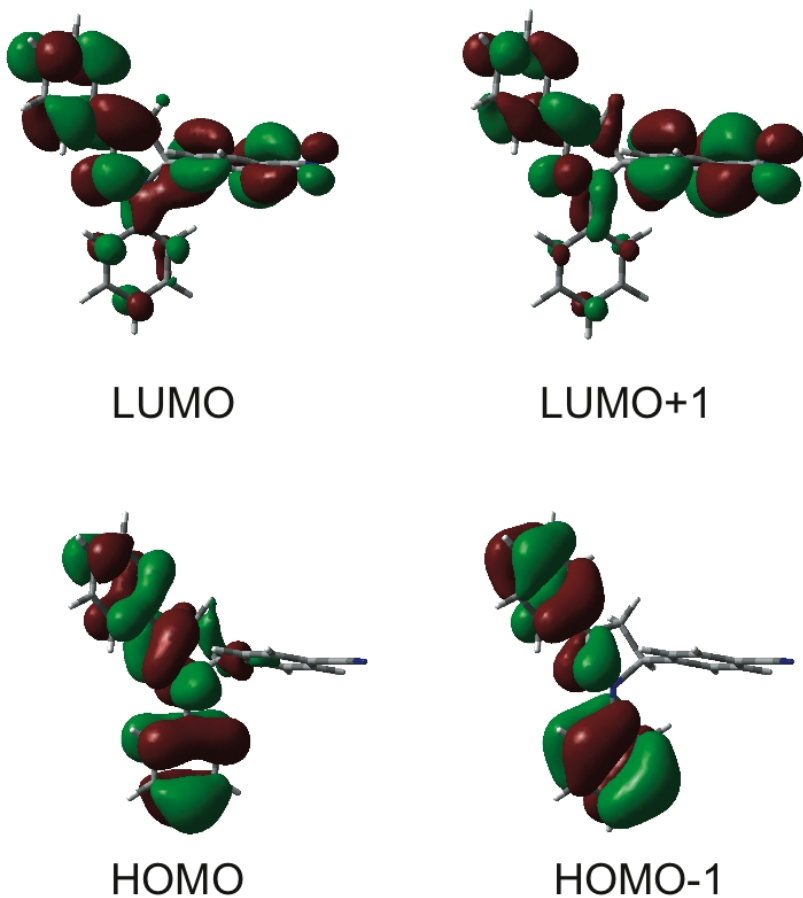


Fig. S18: Frontier molecular orbitals of a Py derivative with a cyanophenyl attached at the C-5 position calculated at the S_1 state geometry. The HOMO and HOMO-1 have no significant density on the cyanophenyl, whereas the LUMO and LUMO+1 are delocalised over the whole molecule.

References

- 1 B. M. Krasovitsky and L. M. Afanasiadi, *Kharkiv, Folio*, 1997, 208.
- 2 I. H. M. van Stokkum, D. S. Larsen and R. van Grondelle, *Biochim. Biophys. Acta, Bioenerg.*, 2004, **1657**, 82–104.
- 3 J. F. Nagle, L. A. Parodi and R. H. Lozier, *Biophys. J.*, 1982, **38**, 161–174.
- 4 A. Weller, *Z. Phys. Chem. Neue Fol.*, 1982, **133**, 93–98.
- 5 J. T. Edward, *J. Chem. Educ.*, 1970, **4**, 261–270.
- 6 F. Pragst, *J. Prakt. Chem.*, 1973, **315**, 549–564.
- 7 W. N. Greig and J. W. Rogers, *J. Electrochem. Soc.*, 1970, **117**, 1141–1145.
- 8 C. V. Stevani, S. M. Silva and W. J. Baade, *Eur. J. Org. Chem.*, 2000, **2000**, 4037–4046.
- 9 T. Förster, *Ann. Physik*, 1948, **2**, 55–75.
- 10 T. Pullerits, S. Hess, J. L. Herek and V. Sundström, *J. Phys. Chem. B*, 1997, **101**, 10560–10567.